



Effect of Sensitizing Treatment on the Microstructure and Susceptibility to Intergranular Corrosion of High-Nitrogen Austenitic Stainless Steel

Wenqian Zhou¹ · Weiwei Ma¹ · Yamin Li¹ · Yufu Sun²

Received: 10 September 2020 / Revised: 12 November 2020 / Accepted: 20 November 2020 / Published online: 6 January 2021
© ASM International 2021

Abstract

This experiment investigated the effect of different sensitizing treatment times (2–48 h) at 800 °C on the microstructure and intergranular corrosion of high-nitrogen austenitic stainless steel by using scanning electron microscopy, energy-dispersive spectroscopy, double loop electrochemical potentiokinetic reactivation, and an oxalic acid etch test. The results indicate that with increasing sensitizing time, the austenite grains grew significantly and the carbide quantity began to increase at the grain boundary. The lamellar pearlite-like Cr₂N was precipitated when the specimens were aged at 800 °C for 12 h. DL-EPR testing showed that IGC susceptibility of high-nitrogen austenitic stainless steel is mainly caused by the precipitation of carbide and increases when sensitization time is increased from 2 to 48 h.

Keywords High-nitrogen austenitic stainless steel · SEM · EDS · DL-EPR · Intergranular corrosion

Introduction

High-nitrogen austenitic stainless steels (ASSs) can be defined as steels that contain more than 0.4 % (mass percent) nitrogen in an austenitic matrix; they are largely used in construction industries due to their superior combination of mechanical, fabrication, and corrosion resistance properties in very aggressive environments [1–3]. However, they are subject to localized corrosion problems such as intergranular corrosion (IGC), pitting corrosion, and stress corrosion cracking. Among these forms of corrosion, IGC is widely encountered for most stainless steels [4–6] and may occur due to the sensitization that results from heat treatment and welding processes, which are carried out at temperatures ranging from 600 to 1000 °C [7].

A sensitized ASS could result from chromium carbide precipitation, which creates chromium-depletion zones adjacent to grain boundaries [8, 9]. The grain boundaries along the chromium-depletion zones favor electrochemical dissolution in certain environments, leading to localized IGC attack along the grain boundaries, which can result in loss of material strength, loss of performance or changes in other desired material properties [10–12]. Several attempts have been made to improve the performance of the material and increase the resistance of stainless steel to IGC corrosion [13]. It is generally believed that some beneficial elements such as chromium, nickel, molybdenum, and nitrogen increase IGC resistance. At the same time, the element of nitrogen added to austenitic steel also draws great attention from engineers and researchers [14]. According to the current research, the addition of nitrogen can be justified as follows: (1) occurrence of the nitrogen consumption mechanism, whereby nitrogen dissolves and binds with H⁺ to reduce the content of H⁺ in the grain boundary; (2) nitrogen can promote the formation of a passive film, which provides good corrosion resistance properties [15, 16].

Over the past few decades, several typical tests have been developed to evaluate the susceptibility of sensitized stainless steels to IGC. For example, electrochemical impedance spectrum and electrochemical noise techniques have been employed to assess the intergranular corrosion in austenitic

✉ Yufu Sun
yufusun@zzu.edu.cn
Wenqian Zhou
18790270529@163.com

¹ School of Mechanical and Electrical Engineering, Xinlian College of Henan Normal University, Zhengzhou 451400, China

² School of Materials Science and Engineering, Zhengzhou University, 97 Wenhua Road, Zhengzhou 450002, China

steels. In addition, electrochemical potentiokinetic reactivation (EPR) methods also can successfully detect the degree of sensitization in stainless steels by measuring the reactivation associated with chromium depleted areas of the lamellar constituent with advantages such as being rapid, quantitative, non-destructive, and valid for in situ measurements [17, 18].

In the past few years, more attention has been devoted to stainless steels like tin-added ASS, super ASS, duplex stainless steel, and so on. Few attempts, however, have been made to clarify the relationship between microstructure evaluation and IGC susceptibility of high-nitrogen ASS.

The aim of the current research is to investigate the effect of sensitizing treatment on the microstructure and susceptibility to intergranular corrosion of high-nitrogen austenitic stainless steel, providing the fundamental knowledge for the further development of evaluations on susceptibility to IGC.

Experimental Procedure

Sample Preparation and Heat Treatments

The materials used in this work were provided by Jiyuan Petroleum Machinery Equipment Co. LTD, with 0.49 wt. % nitrogen at based of ASS. The chemical composition was obtained by spectrometry of ASS, as shown in Table 1. The experimental samples were cut into 10×10 mm pieces from block steel with a thickness of 5 mm. All the samples were solution treated at 1100 °C for 2 h in N₂ flow then water-quenched to room temperature. For detecting the effect of sensitization treatment on microstructural changes that can influence IGC susceptibility, those samples were then subjected to sensitization treatment by heating to a temperature of 800 °C under a stream of argon for 2, 4, 6, 12, 24, and 48 h and then air-cooled. All of these samples were referred to as “aged specimens.”

Samples for metallography were prepared using a traditional method: roughed by abrasive paper (the particle sizes were 100, 200, 400, 600, 800, and 1200) and polished using chromium oxide polish solution. After etching with 50 % HNO₃ + 50 % HCl (wt.%), the microstructure of aged specimens sensitized for different times was observed with a Leica DM4000M optical microscope (OM). Afterward, a FEI-Quanta-200 scanning electron microscopy (SEM) equipped with energy-dispersive spectroscopy (EDS) was used to observe the distributions of different elements at this stage, as well as the precipitate.

Double Loop Electrochemical Potentiokinetic Reactivation (DL-EPR) Test

DL-EPR was performed using a Princeton PARSTAT M electrochemical system, using a conventional three-electrode cell. The samples were used as the working electrodes, which were embedded in epoxy resin leaving a working area of 10×10 mm. Subsequently, all samples were polished and cleaned by ethanol and deionised water prior to tests. Platinum foil and a saturated calomel electrode (SCE) were used as the counter and reference electrodes, respectively. The electrolyte was 0.8 M H₂SO₄ + 0.8 M HCl + 0.01 M KSCN, and the temperature was 25±1 °C. During the DL-EPR test, the working electrode was immersed into solution for 10 min until the steady-state open circuit potential (E_{OCP}) was reached. Afterward, the working electrode was anodically polarised at a scanning rate of 1.667 mV/s from E_{OCP} to a potential of 300mV versus SCE. Then, the scanning direction was reversed back to E_{OCP} at the same scan rate. After each test, microstructure analysis was carried out using an OM to evaluate the region and degree of IGC attack.

For each test, at least 3 time measurements were performed to ensure its reproducibility and samples were tested as standardized in GB/T 29088-2012 [19]. In forward scanning, the peak current (I_a) of the anode could be measured by dissolving the whole sample surface and the peak reaction current (I_r) could be obtained during reverse scanning due to the precipitation of chromium carbide in ASS causing the active dissolution of the chromium-depletion zone at the grain boundary. The ratio of current density $R=I_a/I_r$ is defined as sensitization.

Oxalic Acid Etch Test

All specimens were dipped into 10 % oxalic acid solution at 1 A/cm² for different times (15, 30, 60, and 90 s) according to GB/T 4334.1-2000 [20]. During the etch test, the specimens were made as anode and a stainless steel cup with 10 % oxalic acid solution was used as cathodic. For each test, the solution was replaced with a new solution. After the oxalic acid test, etched surfaces were rinsed with flowing water and alcohol and then dried. The microstructures were observed using an OM, and the etched structures were classified as step, dual, and ditch.

Table 1 Final chemical composition of austenitic stainless steel (wt.%)

C	Si	Mn	S	P	Ni	Cr	Mo	Cu	N
0.012	0.53	20.46	0.006	0.019	1.85	17.9	0.51	0.04	0.49

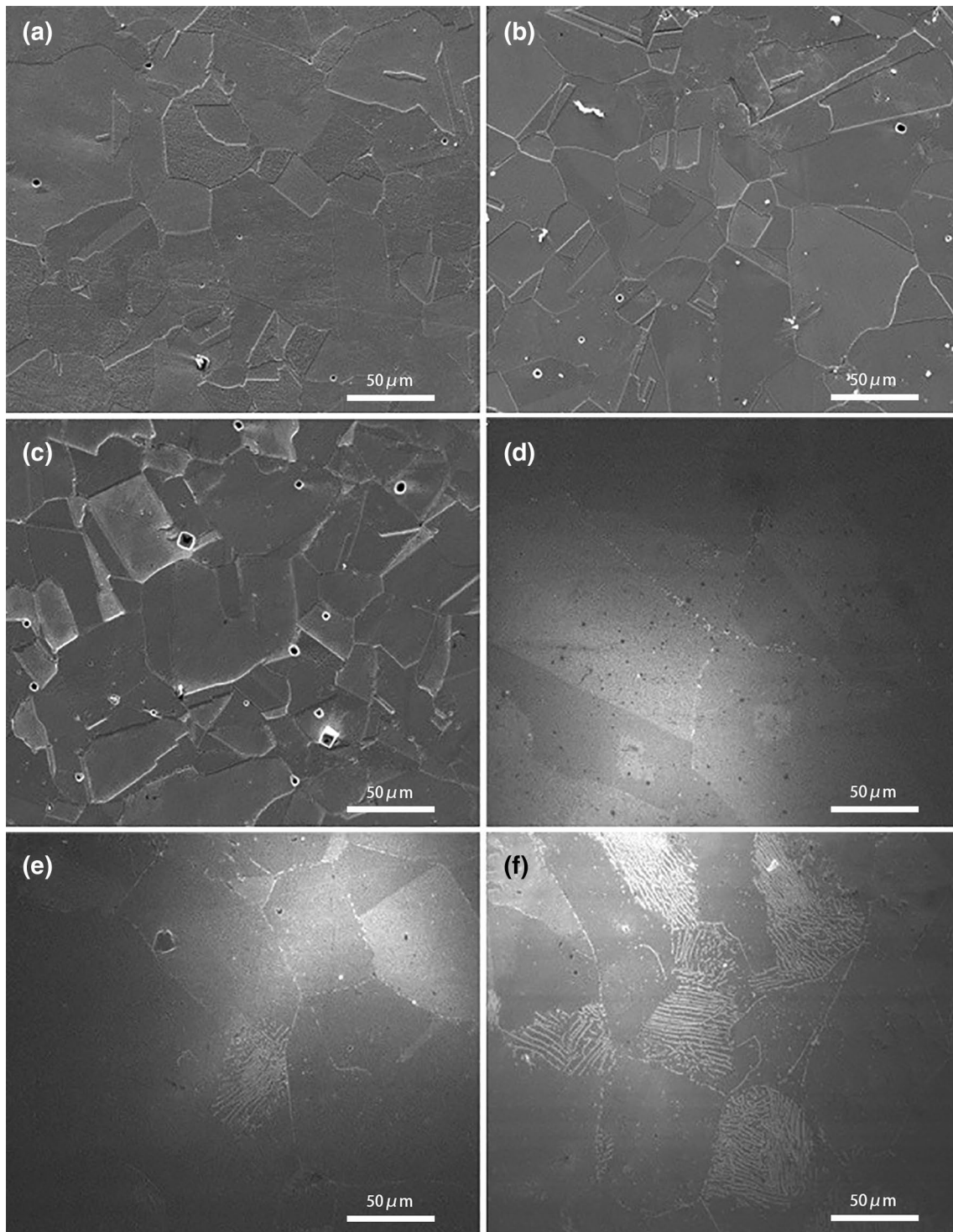


Fig 1 The SEM images of austenitic stainless steel after solution and sensitization heat treatment at 800 °C for different time (a) 2 h (b) 4 h (c) 6 h (d) 12 h (e) 24 h (f) 48 h.

Result and Discussion

Microstructure Observation

Figure 1 shows SEM images of the microstructure of samples sensitized at 800 °C for different times. From Fig. 1, it can be seen that the microstructure largely consists of single austenite and the grain size of austenite increases obviously with the increasing sensitizing time. For longer sensitizing times, precipitated phases in metal matrix can be observed at the edge and center of the samples. It should be noted that the metal matrix shown in Fig. 1d, e and f may be the same, while the morphologies and the amount of precipitated phase are totally different to each other. Tiny and granular precipitate begins to appear at the austenite boundary (Fig. 1d), and then, the amount of granular precipitate increases and the lamellar pearlite-like microstructure of the particles begins to appear in the austenite crystal (Fig. 1e) with increasing sensitizing time. It can clearly be seen that the amount of precipitate gradually increases and the distribution is denser. Some of the lamellar precipitates even fill the entire crystal grains when the samples are sensitized for 48 h (Fig. 1f).

The change process of precipitates in the process of sample sensitization is relatively complicated. Firstly, precipitation occurs not only at the grain boundary but also at the intracrystalline boundary. With the increase in sensitization time, the precipitates gradually increase and the morphology of precipitates also changes. As shown in Fig. 1e, when sensitized for 24 h, the morphology of the precipitate changes from the original scattered particles to thin strips and lamellae. The samples of high-nitrogen ASS are desolvating precipitation during the sensitization process. These precipitates will preferentially grow up in high energy areas such as grain boundaries and dislocations. With the extension of sensitization time, precipitates will aggregate into the crystal and will also appear at the intracrystalline.

In order to analyze the elemental composition and content of precipitates in ASS after sensitization, EDS was used for area scanning and point energy spectrum analysis on the samples; the results are shown in Fig. 2.

It can be seen from Fig. 2 that the precipitate of high-nitrogen ASS sensitized at 800 °C for 48 h has a lamellar morphology, in which Mn, Cr, N, C, and Si elements are uniformly distributed in the matrix, while the content of Cr and N elements in the precipitate is relatively high. In order to further analyze the composition of elements in the precipitates, the ASS matrix and precipitates were analyzed by EDS and the results are revealed in Fig. 3.

In Fig. 3, Spectrogram 1 is the energy spectrum of granular precipitates in grain boundaries, Spectrogram 2 is the

energy spectrum of massive precipitates in grain boundaries, Spectrogram 3 is the energy spectrum of lamellar precipitates at intracrystalline, and Spectrogram 4 is the energy spectrum of the matrix near grain boundaries.

From Figure 3 and Table 2, it can be concluded that the precipitates contain more Cr and Mn, indicating that the precipitates in the sensitization process of stainless steel are Cr_2N , M_{23}C_6 , and intermetallic compounds, and the lamellar precipitates of pearlite-like structure contain higher N element, so the lamellar precipitates are Cr_2N . Zou Zhangxiong et al. [21] found that Cr_2N precipitated in 0.7N38K ASS is a typical pearlite-like structure when sensitized at 800 °C. As nitrogen is an active element in the interface, it is easy to agglomerate toward the grain boundary. The nitrogen is easily able to form Cr_2N with chromium and precipitate on the grain boundary at a suitable sensitization temperature. The higher the nitrogen content, the more obvious this trend is and the easier the nitride precipitates. In addition, the type and morphology of precipitates are not only related to the holding time, but also to the nitrogen content and alloy element content in ASS.

EDS results in Table 2 show that the chromium content (34 %) in the energy spectrum results of intragranular massive nitrides is relatively high, while the chromium content (10.75 %) in the matrix near the grain boundary is relatively low, which indicates that a chromium-depletion area has been formed around the nitrogen carbide precipitates. The formation and growth of the chromium-rich phase and M_{23}C_6 and other carbonitrides affects the distribution of alloy elements in local areas. For example, chromium, manganese, and iron near the matrix carbonitride interface at the grain boundary change with the formation of precipitates. According to the research of Jainf [22], if the chromium content in the local area at the grain is less than 12 %, the chromium-depletion area will easily produce local serious IGC in the corrosive medium environment. In addition, with the extension of sensitization time, the chromium content returns to the original content due to diffusion from the matrix to the carbonitride-grain boundary interface to prevent the formation of chromium-depletion areas at grain boundaries, but this sensitization time is long and is not taken as a heat treatment measure to eliminate the chromium-depletion areas.

Oxalic Acid Etch Test Results

Figure 4 reveals the corrosion morphology of sensitized stainless steel after the oxalic acid etch test for different times. From Fig. 4, the degree of IGC increases with an increase in etching time in 10 % oxalic acid solution. The specimen etched for 15 s exhibits a slight IGC attack with a dual structure, mixed with step and ditch structures. The specimens etched for 60 and 90 s are classified as the ditch structure, and all the grains are completely encircled

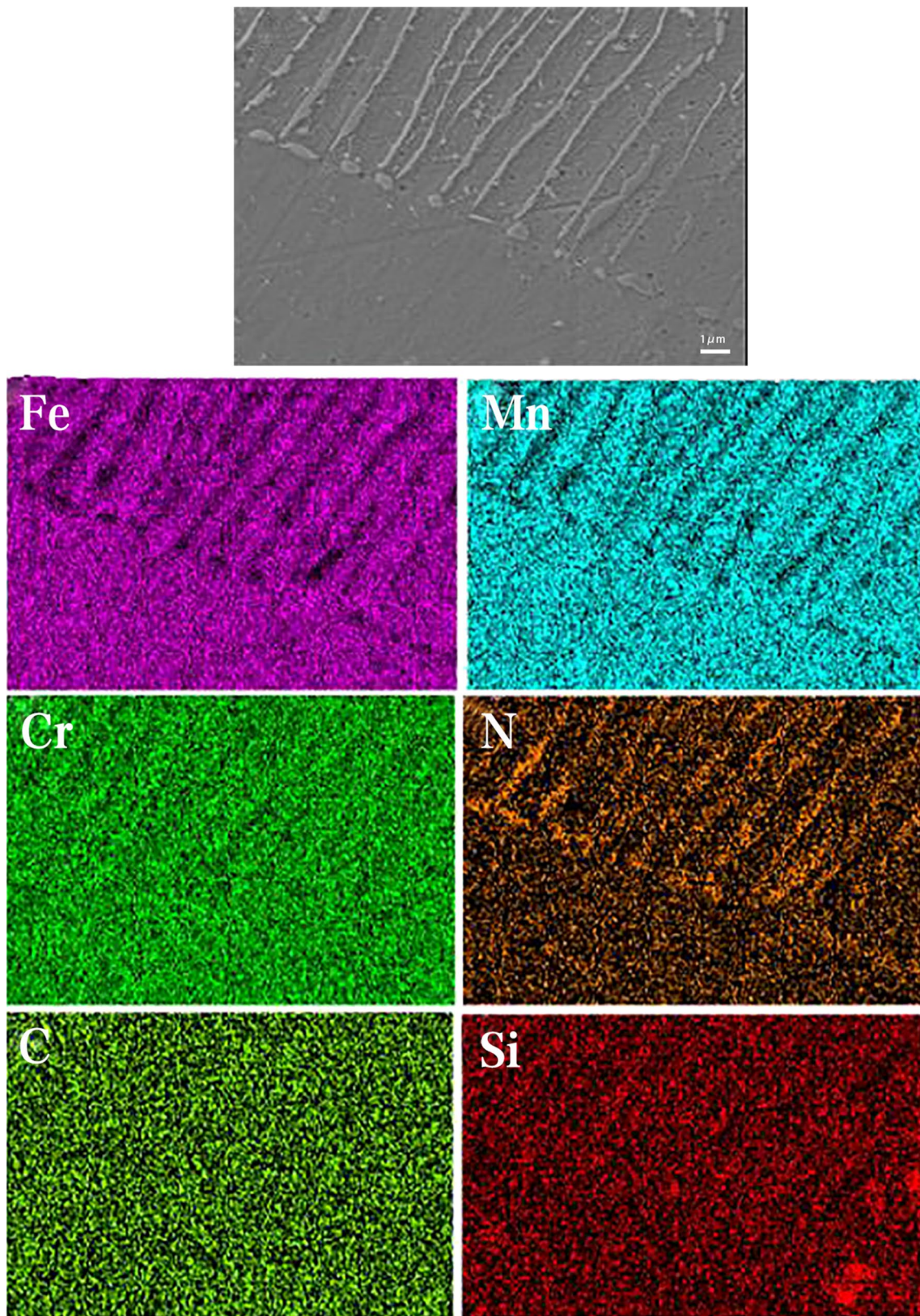


Fig 2 Scanning image of precipitates after solution and sensitization heat treatment at 800 °C for 48 h and results of area scanning of the main elements

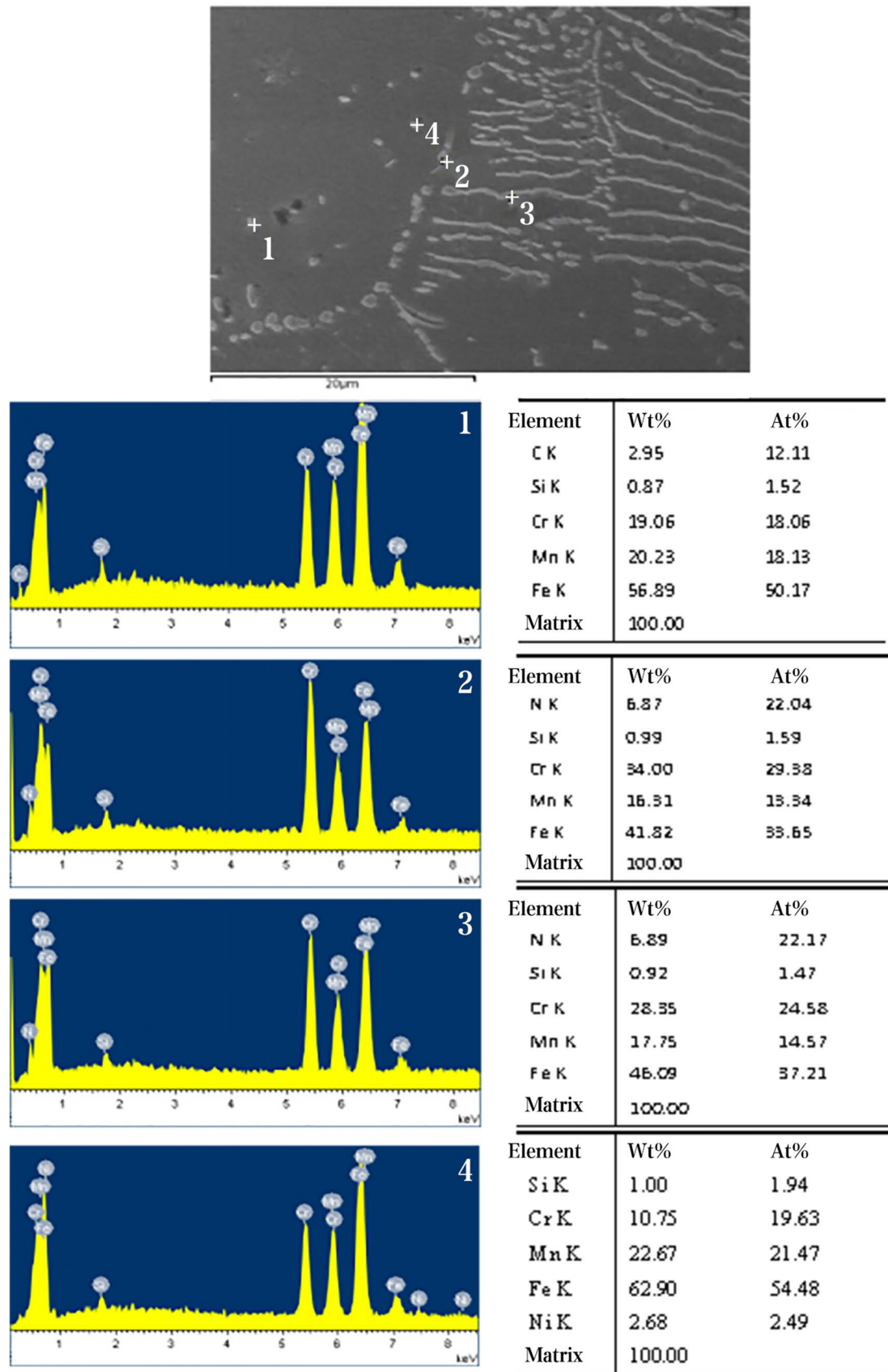
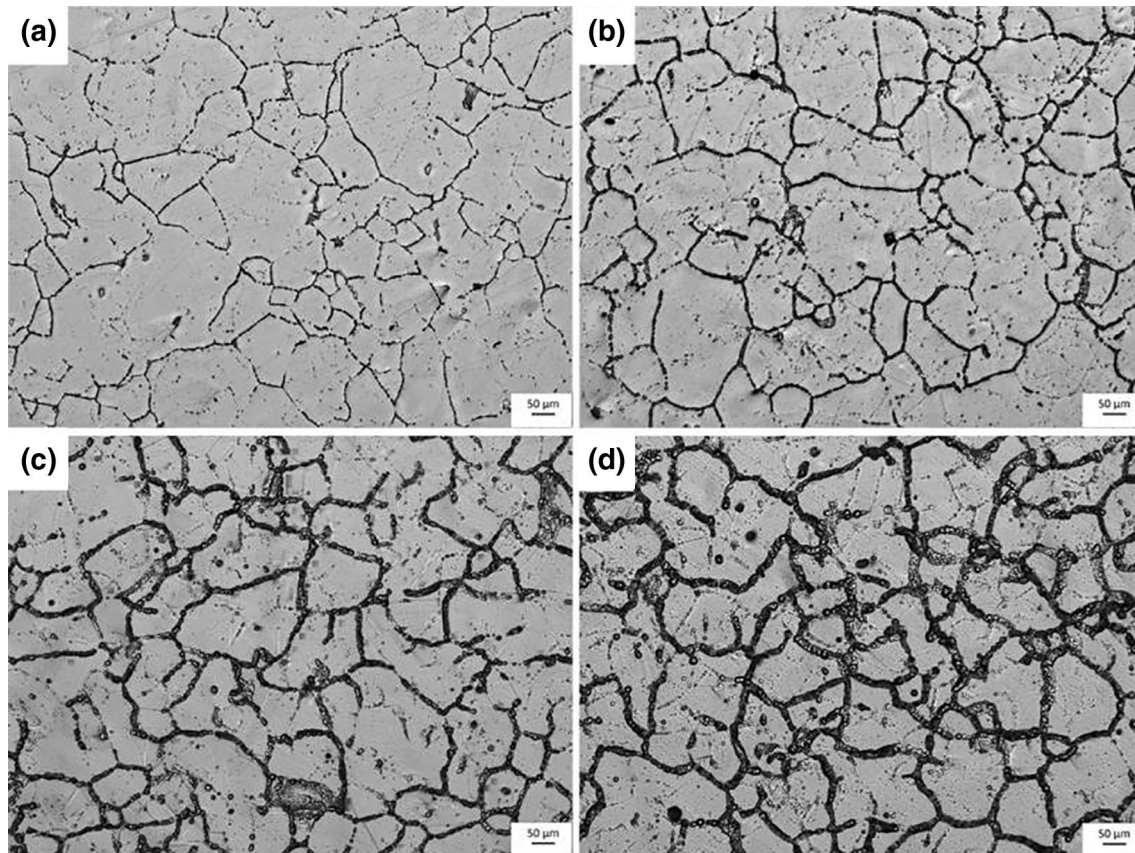


Fig 3 The results of EDS analysis of specimen after solution at 800 °C and sensitization for 48 h.

Table 2 Analysis of Main Elements of Precipitates after sensitization at 800 °C for 48h

Element	C	N	Cr	Mn	Si	Fe
Matrix near grain boundary	10.75	22.64	1.00	62.9
Granular precipitates	2.95	...	19.06	20.23	0.87	56.89
Massive precipitates	...	6.87	34	16.31	0.99	41.82
Lamellar precipitates	...	6.89	28.35	17.75	0.92	46.09

**Fig 4** Corrosion morphology of sensitized stainless steel in oxalic acid after galvanostatic etching for different time (a) 15 s (b) 30 s (c) 60 s (d) 90 s.

by etched grain boundaries, characteristic of completely sensitized materials. Meanwhile, the degree of IGC in the specimens etched for 90 s is obviously more severe than the other three specimens. When constant-current etching of sensitized stainless steel is performed in oxalic acid solution for different periods of time, slight corrosion occurs at first due to the poor stability of the passivation film in the chromium-depleted region of stainless steel at the beginning of the etch test. The chromium zone gradually dissolves and presents the characteristics of IGC. As a result, the development of intergranular corrosion depends on the etching time.

DL-EPR Test Results

Figure 5 shows the typical DL-EPR curves for specimens after sensitization heat treatments for different times, and the variation of the degree of sensitization of specimens is shown in Table 3. From Fig. 5, it could be seen that the EPR curves of the samples treated with different sensitization times show typical activation peaks and reactivation peaks. As shown in Fig. 5a, the activation peak of the sensitized 2 h sample differs greatly from that of the sensitized 4 h sample. As shown in Fig. 5b, when the sensitization time is 12, 24 and 48 h, the difference of each peak value on the curve is

Fig 5 DL-EPR curves for samples after sensitization at 800 °C for different time (a) 2 h, 4 h and 6 h (b) 12 h, 24 h and 48 h

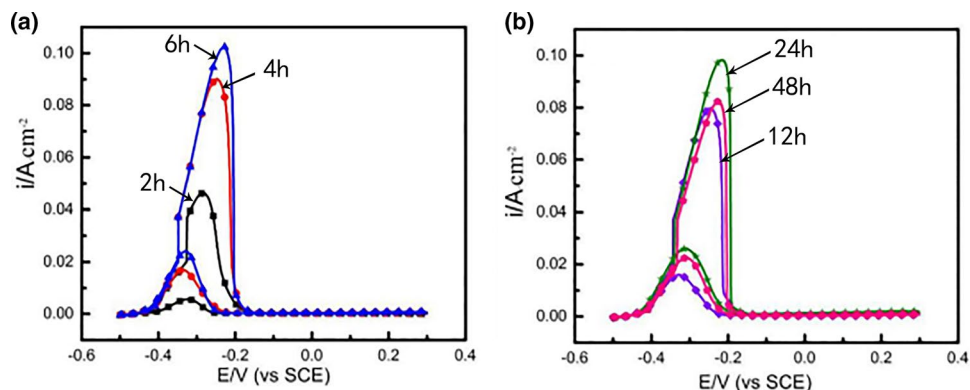


Table 3 Reactivity R of sample after sensitization at 800 °C for different time after DL-EPR test

Sensitization time (h)	Reactivation rate (R)
2	0.113
4	0.167
6	0.199
12	0.235
24	0.264
48	0.272

not very large, which corresponds to the reactivation rate of different treated samples in Table 3. From Table 3, it can be found that the reactivation rate of the samples increases with the extension of sensitization time. The results show that the IGC sensitivity of the sample increases with the increase in sensitization time.

Figure 6 shows SEM images after EPR tests for specimens with sensitizing for different times at 800 °C. From Fig. 6a, the grain boundary of ASS appears slightly after sensitization for 2 h and EPR testing. After corrosion, the grain boundaries of the samples sensitized for 6 h have been significantly thickened. After the sample with sensitization time of 12 h is corroded, the grain boundaries have been connected into a network, which indicates that the precipitation of carbonitride has been sufficient and the material has suffered serious IGC. With the extension of sensitization time, precipitates on grain boundaries have increased obviously, showing typical IGC characteristics. As shown in Fig. 6f, when the sensitization time is 48 h, the grain boundaries are all connected into a net shape and the corrosion grooves are deeper compared with the previous ones.

Figure 7 shows the relationship between calculated R_a values and sensitization time. The reactivation rate

increases rapidly with the extension of the sensitization time when the sensitization time is less than 12 h, while the reactivation rate increases slowly with the continuous increase in the sensitization time. In the sensitization process of stainless steel, $M_{23}C_6$, Cr_2N and σ phases are equal at the grain boundary, resulting in chromium-depletion areas at the austenite grain boundary. In the early stages, the formed $M_{23}C_6$, Cr_2N , and σ increase with the increase in sensitization time and the chromium-depletion areas become more pronounced, leading to a rapid increase in IGC susceptibility with the increase in sensitization time. However, as the diffusion rate of chromium atoms is less than that of carbon atoms, the formation rate of $M_{23}C_6$, Cr_2N , etc., is limited by the content of carbon and nitrogen at the grain boundary as sensitization progresses. Meanwhile, chromium atoms diffuse from inside the grain to the grain boundary to fill up the chromium-depletion area, and the IGC sensitivity of the samples slowly increases [23].

Conclusion

The major conclusions derived from the present investigations are:

- (1) IGC resistance of high-nitrogen ASS can be strongly affected by microstructural changes induced by sensitizing treatments. When high-nitrogen ASS is sensitized at 800 °C for different times, the austenite grain size gradually increases with the increase in sensitization time and the morphology and quantity of precipitates also change. When the sensitization time is 12

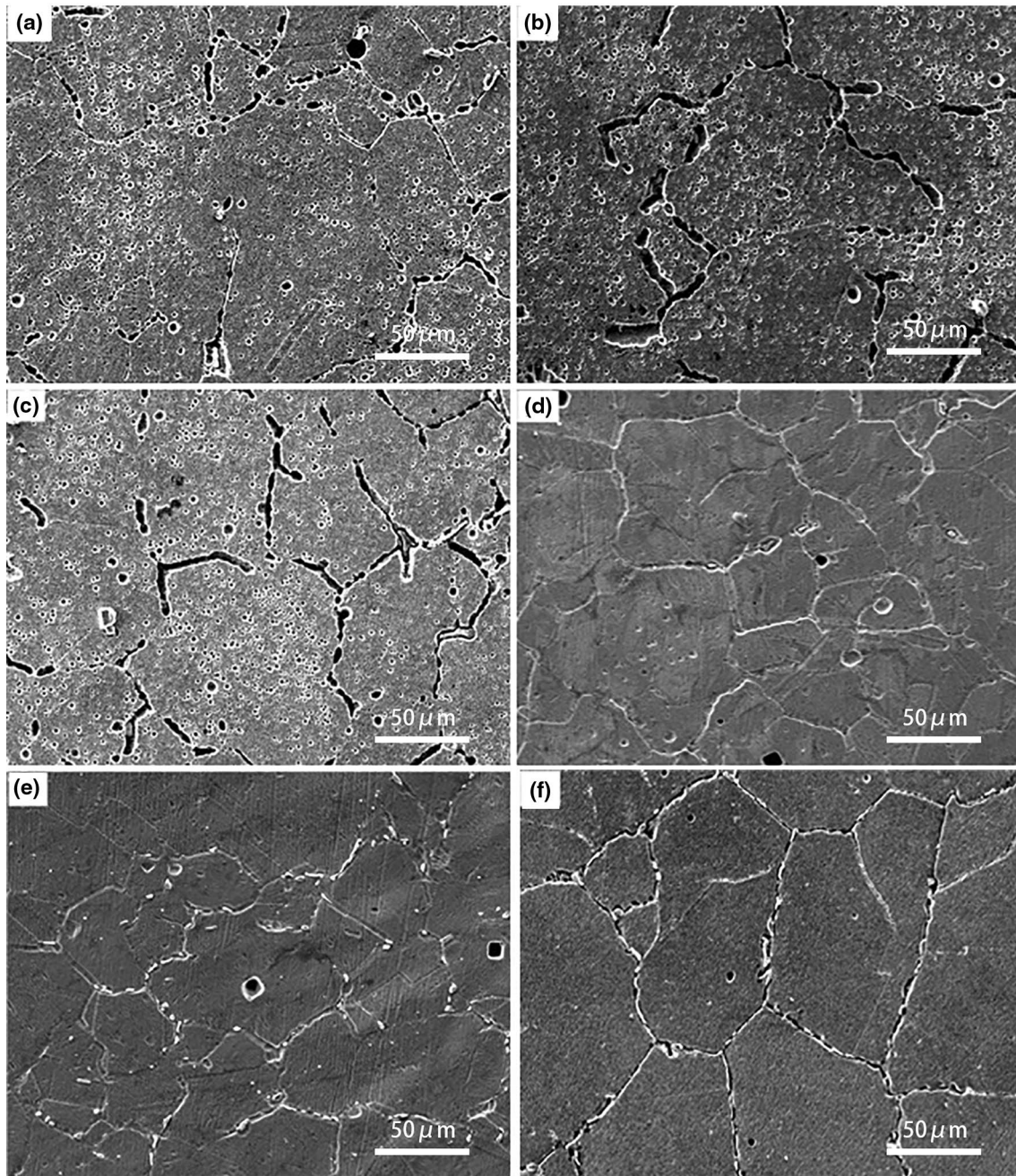


Fig 6 Morphologies of specimen with sensitizing at 800 °C for different time after EPR test (a) 2 h (b) 4 h (c) 6 h (d) 12 h (e) 24 h (f) 48 h

h, Cr_2N with a lamellar pearlite-like structure, M_{23}C_6 begins to precipitate in the grains and can cause chromium-depletion zone at grain boundaries and increase the IGC susceptibility of this steel.

(2) The reactivation rate of samples sensitized at 800 °C for different times increases with the increasing sensitization time and the IGC sensitivity of samples also increases with the increase in sensitization time.

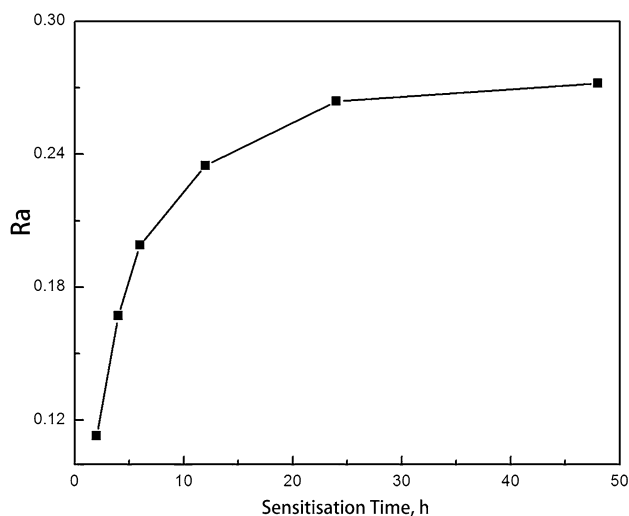


Fig 7 The relationship between sample reactivation and sensitization time

Acknowledgements We would like to thank the Science and Technology Program of Henan Province (Project No. 182102210083) for the opportunity to carry out this work.

References

1. A.I. Munoz, J.G.A. Anton, J.L. Guinon, V.P.R. Herranz, A.I. Munoz, J.G.A. Anton, J.L. Guinon, V.P.R. Herranz, Inhibition effect of chromate on the passivation and pitting corrosion of a duplex stainless steel in LiBr solutions using electrochemical techniques. *Corros. Sci.* **49**, 3200–3225 (2007)
2. H. Sidhom, T. Amadou, C. Braham, H. Sidhom, T. Amadou, C. Braham, Evaluation by the double loop electrochemical potentiokinetic reactivation test of aged ferritic stainless steel intergranular corrosion susceptibility. *Metall. Mater. Trans. A.* **41**, 3136–3150 (2010)
3. S. Frangini, A. Mignone, S. Frangini, A. Mignone, Modified electrochemical potentiokinetic reactivation method for detecting sensitization in 12 wt% Cr ferritic stainless steels. *Corros. Sci.* **48**(9), 715–726 (1992)
4. S.C. Zhang, Z.H. Jiang, H.B. Li, H. Feng, B.B. Zhang, S.C. Zhang, Z.H. Jiang, H.B. Li, H. Feng, B.B. Zhang, Detection of susceptibility to intergranular corrosion of aged super austenitic stainless steel S32654 by a modified electrochemical potentiokinetic reactivation method. *J. Alloys Compd.* **695**, 3083–3093 (2016)
5. D.Y. Lin, T.C. Chang, D.Y. Lin, T.C. Chang, Influence of Si content on the intergranular corrosion of SUS 309L stainless steels. *Mater. Sci. Eng. A.* **359**(1–2), 396–401 (2003)
6. R. Luo, X.N. Cheng, D.S. Li, G.F. Xu, P. Gao, S. Guo, Y. Qiu, Q. Zheng, R. Luo, X.N. Cheng, D.S. Li, G.F. Xu, P. Gao, S. Guo, Y. Qiu, Q. Zheng, Research on intergranular corrosion of welded joint of nuclear-grade austenitic stainless steel. *J. Funct. Mater.* **45**(23), 23033–23037 (2014)
7. A. Kriaa, N. Hamdi, H. Sidhom, A. Kriaa, N. Hamdi, H. Sidhom, Assessment of intergranular corrosion of heat treated austenitic stainless steel (AISI 316L Grade) by electron microscopy and electrochemical tests. *Prot. Met. Phys. Chem. Surf.* **44**(5), 506–513 (2008)
8. A.Y. Kina, V.M. Souza, S.S.M. Tavares, J.A. Souza, H.F.G. de Abreu, A.Y. Kina, V.M. Souza, S.S.M. Tavares, J.A. Souza, H.F.G. de Abreu, Influence of heat treatments on the intergranular corrosion resistance of the AISI 347 cast and weld metal for high temperature services. *J. Mater. Process. Technol.* **199**, 391–395 (2008)
9. T. Amadou, C. Braham, H. Sidhom, T. Amadou, C. Braham, H. Sidhom, Double loop electrochemical potentiokinetic reactivation test optimization in checking of duplex stainless steel intergranular corrosion susceptibility. *Metall. Mater. Trans. A.* **35**, 3499–3513 (2004)
10. Y.J. Oh, J.H. Yoon, J.H. Hong, Y.J. Oh, J.H. Yoon, J.H. Hong, Carbon and nitrogen effects on sensitization resistance of type 347 stainless steels. *Corros. Houston Tx.* **56**(3), 289–297 (2000)
11. Y.J. Oh, B.S. Lee, J.H. Hong, B.J. Lee, O. Yoo, Y.J. Oh, B.S. Lee, J.H. Hong, B.J. Lee, O. Yoo, Precipitation behavior of carbonitrides in type 347 stainless steels with various C and N contents. *Metall. Mater. Trans. A.* **33**(5), 1565–1569 (2002)
12. X.Z. Huang, D. Wang, Y.T. Yang, X.Z. Huang, D. Wang, Y.T. Yang, Effect of precipitation on intergranular corrosion resistance of 430 ferritic stainless steel. *J. Iron. Steel Res. Int.* **22**(11), 1062–1068 (2015)
13. C.J. Scheuer, F.A.A. Possoli, P.C. Borges, R.P. Cardoso, S.F. Brunatto, C.J. Scheuer, F.A.A. Possoli, P.C. Borges, R.P. Cardoso, S.F. Brunatto, AISI 420 martensitic stainless steel corrosion resistance enhancement by low-temperature plasma carburizing. *Electrochim. Acta.* **317**, 70–82 (2019)
14. M. Sun, Y.Y. Yang, M. Luo, L.Z. Jiang, Y.M. Jiang, J. Li, M. Sun, Y.Y. Yang, M. Luo, L.Z. Jiang, Y.M. Jiang, J. Li, Investigation of susceptibility to intergranular corrosion of tin-added austenitic stainless steel. *Acta Metall. Sin. Engl. Lett.* **28**(9), 1183–1189 (2015)
15. Y. Kobayashi, Y. Kobayashi, Fabrication of high strength high nitrogen stainless steel with excellent corrosion resistance and its mechanical properties. *Mater. Manuf. Processes.* **19**(1), 19–30 (2004)
16. G. Lorang, M.D.C. Belo, A.M.P. Simoes, G. Lorang, M.D.C. Belo, A.M.P. Simoes, Chemical composition of passive films on AISI 304 stainless steel. *J. Electrochem. Sci.* **141**(12), 3347–3356 (1994)
17. X.D. Lin, Q.J. Peng, E.H. Han, W. Ke, X.D. Lin, Q.J. Peng, E.H. Han, W. Ke, Assessment of thermal aging of austenitic stainless steel weld metal by using the double loop electrochemical potentiokinetic reactivation technique. *Corrosion.* **75**(4), 377–388 (2019)
18. J.K. Sun, L. Sun, N.W. Dai, J. Li, Y.M. Jiang, J.K. Sun, L. Sun, N.W. Dai, J. Li, Y.M. Jiang, Investigation on ultra-pure ferritic stainless steel 436L susceptibility to intergranular corrosion using optimised double loop electrochemical potentiokinetic reactivation method. *Corros. Eng. Sci. Technol.* **53**(8), 574–581 (2018)
19. GB/T 29088-2012. Corrosion of metals and alloys-Electrochemical potentiokinetic reactivation measurement using the double loop method [S]. China Standard Press.
20. GB/T 4334.1-2000. Method of 10% oxalic acid etch test for stainless steels [S]. China Standard Press.
21. Z.X. Zhang, Y.P. Liang, H.P. Qu, J.Z. Xiang, Z.X. Zhang, Y.P. Liang, H.P. Qu, J.Z. Xiang, Research on microstructure and properties of Cr-Mn-N austenitic stainless steel for non-magnetic drilling collar application. *Hot Work. Technol.* **18**(42), 147–152 (2013)
22. S. Jain, N.D. Budiansky, J.L. Hudson, J.R. Scully, S. Jain, N.D. Budiansky, J.L. Hudson, J.R. Scully, Surface spreading of intergranular corrosion on stainless steels. *Corros. Sci.* **52**(3), 873–885 (2010)

23. P. Forchhammer, H. Engell, P. Forchhammer, H. Engell, Investigation into the pitting corrosion of passive austenitic CrNi steels in neutral chloride solutions. *Werkst. Korros.* **20**, 1 (1969)

Publisher's Note Springer Nature remains neutral with regard to jurisdictional claims in published maps and institutional affiliations.